ADVANCED MATERIALS INTERFACES
www.advmatinterfaces.de

Structural Defects Control the Energy Level Alignment at Organic/Organic Interfaces

*Keiichirou Yonezawa, Alexander Hinderhofer, Takuya Hosokai, Kengo Kato, Rintaro Makino, Frank Schreiber, Nobuo Ueno, and Satoshi Kera**

The dependence of the energy level alignment (ELA) on structural defects at an organic/organic heterojunction (OOH) of perfluoropentacene (PFP)-on-diindenoperylene (DIP) was investigated using X-ray scattering and ultraviolet photoelectron spectroscopy. The density of structural defects near the interface between the PFP and DIP layers was varied by changing the growth temperature of the DIP film. A direct relationship was found between the defect density and the ELA at the OOH; the ELA together with the change in the electrostatic potential (quasi-interface dipole layer) at the OOH varies systematically with the defect density near the interface. This indicates that a key factor affecting the ELA is the electrostatic potential change across the OOH interface, which is produced by electron transfer from DIP occupied gap states to PFP unoccupied gap states. These gap states originate from the defects and are effectively controlled by adjusting the growth conditions of the organic films. As a result, the ELA at OOH interfaces can be controlled by the density of structural defect, which is important for organic devices employing OOHs, such as organic photovoltaic cells.

1. Introduction

The energy level alignment (ELA) at organic-organic heterojunction (OOH) interfaces is crucial for understanding the electrical properties of organic electronic devices, such as organic photovoltaic (OPV) cells and organic light-emitting diodes.[1–4] Especially for OPV cells, the difference in the binding energies (E_b) of the highest occupied molecular orbital (HOMO) of the donor material and the lowest unoccupied molecular orbital (LUMO) of the acceptor material is the key factor for the open-circuit voltage.[5–8] So far, several models have been proposed to explain the ELA mechanism at OOH interfaces. For a precise understanding of the ELA, however, we still need to consider many different factors, not only the inherent electric structure of the involved materials, but also specific intermolecular interactions between the two materials and the contribution of the molecular orientation and/or crystal structure near the interface.[9–21]

We investigated the effect of the density of structural defects at OOH interfaces on the ELA by using X-ray scattering and ultraviolet photoelectron spectroscopy (UPS). We chose prototypical materials relevant for device application: diindenoperylene (DIP, $C_{32}H_{16}$) as a p-type (donor) material (**Figure 1**a) and perfluoropentacene (PFP, $C_{22}F_{14}$) as a n-type (acceptor) material (Figure 1b).[22,23] The density of structural defects at the interface was varied by changing growth temperature (T) of the DIP layers.[22] PFP was deposited step by step on the DIP layer to measure the thickness dependence of the work function (WF) and HOMO positions. The diagrams of the PFP-on-DIP structure shown in Figure 1c illustrate the effect of increased in-plane disorder in the bottom DIP layer on the upper PFP layer.

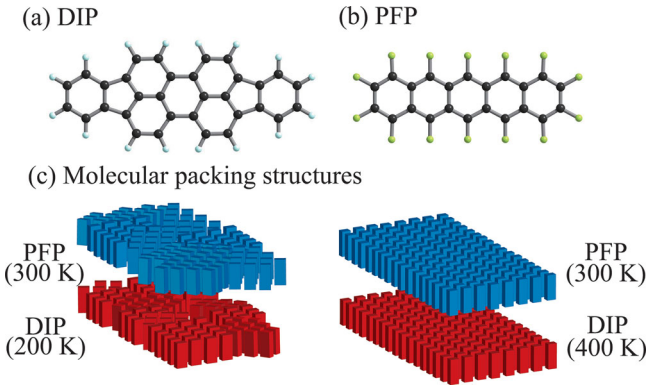

Figure 1. Molecular structures of diindenoperylene (DIP, $C_{32}H_{16}$) (a) and perfluoropentacene (PFP, $C_{22}F_{14}$) (b) and sketch of molecular packing structures controlled by adjusting growth temperature of underlying DIP layer (c).

K. Yonezawa, Dr. A. Hinderhofer, K. Kato, R. Makino, Prof. N. Ueno, Prof. S. Kera
Department of Nanomaterial Science
Graduate School of Advanced Integration Science
Chiba University
1-33 Yayoi-cho, Inage-ku, Chiba 2638522, Japan
E-mail: kera@faculty.chiba-u.jp
Dr. T. Hosokai
Department of Materials Science and Technology
Iwate University
Ueda 4–3–5, Morioka, Iwate 0208551, Japan
Prof. F. Schreiber
Institut für Angewandte Physik
Universität Tübingen
Auf der Morgenstelle 10, Tübingen 72076, Germany

DOI: 10.1002/admi.201400004

© 2014 WILEY-VCH Verlag GmbH & Co. KGaA, Weinheim

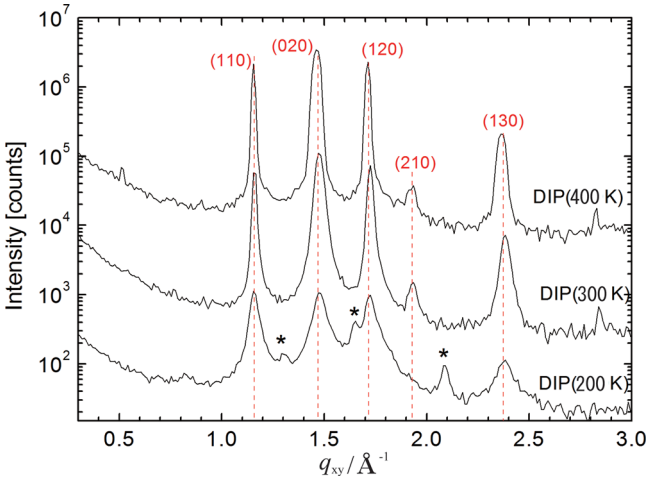

Figure 2. In-plane GIXD data for three DIP layers grown at different substrate temperatures (400, 300, and 200 K) (d_{DIP} = 15 nm). Coherent in-plane island sizes were 32 nm (400 K), and 28 nm (300 K) and 15 nm (200 K). A low-temperature bulk phase was observed in 200-K layer (indicated by '*').

2. Results and Discussion

We first present our structural characterization of the DIP underlayer [thickness (d_{DIP}) = 15 nm]. At growth temperatures of 200 to 400 K, DIP thin films grown on SiO_2 typically exhibit the high-temperature crystal phase (HT phase) and are textured with the (001) plane parallel to the substrate (σ-orientation).[21,24–26] **Figure 2** shows grazing incidence X-ray diffraction (GIXD) data for the three DIP films investigated; the peak indexing is based on the HT phase (P21/a polymorph).[24] The increase in the peak width for lower-*T* films indicates a decrease in the coherent in-plane island size, which can be interpreted as an increase in the structural defects in the film, as confirmed by the present UPS results (see discussion). The coherent island sizes, which were determined from the Scherrer equation, were 32, 28, and 15 nm for 400, 300, and 200 K, respectively. These island sizes indicate that there are much more structure defects in the 200-K film than the 300-K film. At the lowest *T*, 200 K, there are traces of a low-temperature crystal structure, indicated by '*' in Figure 2.[24,27] The amount of this phase was very small and can be neglected for discussion of the UPS spectra.

The main structural difference between the three DIP films grown at different *T*s was the in-plane crystal quality. A detailed study of the growth of PFP on DIP has shown that it exhibits two important effects[22]: (i) PFP molecules evaporated on DIP tend to adopt the nearly standing orientation of the DIP molecules (σ-orientation) (Figure S1); (ii) the in-plane coherent island size of the PFP domains correlates with that of the DIP domains, but the sizes of those in the PFP are larger than those in the DIP (i.e., defects in the DIP template induce defects in the PFP layer (Figure S2), but the defect density in the PFP layer is lower than that in the DIP underneath).

We next discuss the effect of increased defect density on the ELA at the PFP-on-DIP interface. **Figure 3** shows the PFP-thickness dependence of the UPS spectra of three PFP-on-DIP OOHs with the DIP layer grown at three substrate temperatures: 400, 300, and 200 K. The disappearance of the DIP HOMO peak after the deposition of a nominally 3.2-nm-thick PFP layer indicates that the DIP surface was fully covered by the PFP for all the DIP films (confirmed by metastable atom electron spectroscopy; results not shown). Upon PFP deposition, no new peak was observed in the band gap region, indicating that no significant formation of a charge-transfer complex and/or chemical reaction between the DIP and PFP occurred at the interface. The mean value of the HOMO ionization energy (IE) of the three DIP films, determined from the energy difference between the peak maximum of the HOMO and the secondary electron cut-off (SECO), was 5.68 ± 0.03 eV. The mean IE of the HOMO of three 3.2-nm PFP films was 6.92 ± 0.01 eV, after deconvolution of the UPS bands with Gaussian functions (see **Figure 4**). This IE corresponds well with previously reported values for standing DIP and PFP films.[28–30] The growth-*T* independence of the HOMO IE for the DIP films and for the PFP films on the DIP films confirms that there was only a negligible amount of lying or tilted DIP and PFP molecules because organic films with different molecular orientations exhibit different IEs.[17,21,28,30] On the other hand, no systematic dependence of the DIP HOMO E_b on the defect density was observed, which possibly due to an uncontrollable variation in the WF of the SiO_2 substrates (see Figure S3).

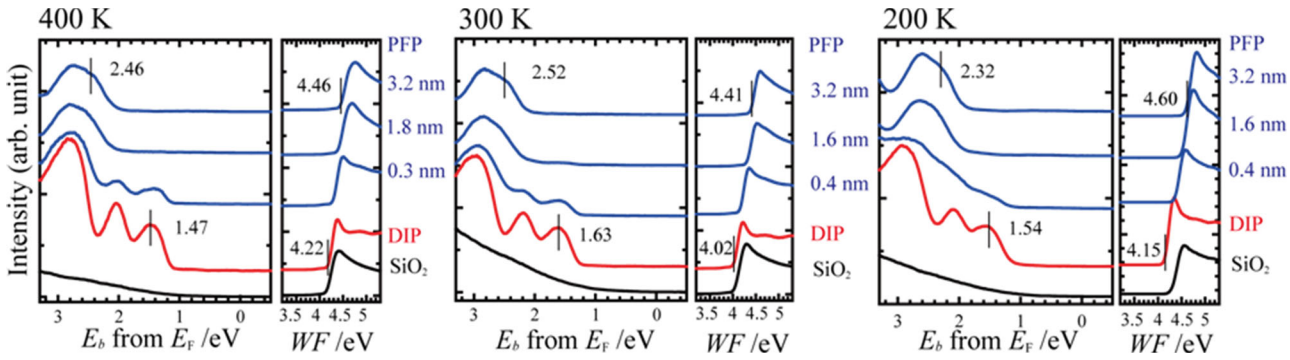

Figure 3. UPS spectra of PFP-on-DIP on SiO_2 (DIP growth *T* = 400, 300, and 200 K): from bottom to top, SiO_2 (black), 15 nm DIP (red), and PFP thickness dependence (blue). Binding energies of each HOMO peak and onset positions of SECO (work function/WF) are given in eV.

© 2014 WILEY-VCH Verlag GmbH & Co. KGaA, Weinheim

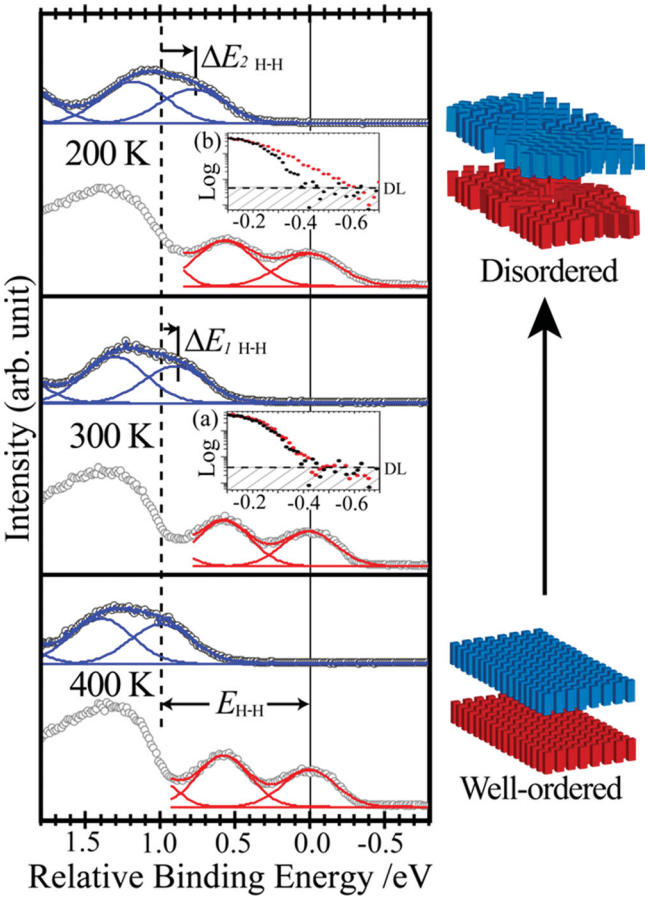

Figure 4. Comparison of UPS spectra of DIP films deposited on SiO_2 substrate at different temperatures (400, 300, and 200 K) with those of PFP (3.2 nm) on those three DIP films. All spectra were aligned relative to the DIP HOMO peak. $E_{H\text{-}H}$ is energy difference between DIP and PFP HOMOs for PFP on 400-K DIP film. $\Delta E_{1H\text{-}H}$ ($\Delta E_{2H\text{-}H}$) is change in PFP HOMO position from that on the 400-K DIP film for PFP film on the 300-K (200-K) DIP film. Spectra were fitted using Gaussian functions. FWHM of DIP HOMO was 0.41 eV (400 K), 0.42 eV (300 K) and 0.48 eV (200 K), and FWHM of the PFP HOMO was 0.50 eV, 0.50 eV and 0.51 eV for PFP films on 400-, 300-, and 200-K DIP films, respectively. Insets (a) and (b) show 300-K and 200-K spectra on log scale for the intensity of DIP HOMO including the tailing region, respectively. The black dots correspond to the spectrum (density of states) of 400-K DIP HOMO and the red dots to that at the lower temperature, indicating increase in the intensity (density of states) caused by the structural defects. The dashed line in each inset is the detection limit (DL) of the present UPS.

Figure 4 shows the UPS spectra of DIP and PFP (3.2 nm)-on-DIP films (T = 400, 300, and 200 K). All the spectra were aligned relative to the DIP HOMO peak after Gaussian deconvolution of the DIP (red pattern) and PFP (blue pattern) HOMO peaks to discuss phenomena at the PFP-DIP interface. The full-width at half maximum (FWHM) of the DIP HOMO was 0.41, 0.42, and 0.48 eV for 400-, 300-, and 200-K DIP films, respectively, and that of the PFP HOMO is 0.50, 0.50, and 0.51 eV on the 400-, 300-, and 200-K DIP films, respectively. Note that the FWHM of the DIP HOMO increased with a decreasing DIP growth temperature, which suggested an increase in the density of gap states (DOGS). The DOGS increase was confirmed by the spectra on log intensity scale for 300-K [Figure 4 inset (a)] and 200-K [Figure 4 inset (b)] DIP films for the HOMO tailing region with comparison with that for 400-K DIP film, where contribution of photoelectrons excited by HeIβ (hν = 23.08 eV) is subtracted. The results clearly demonstrate an increase in the DOGS in particular for the 200-K film due to the increase in structural defects, being in good agreement with the difference among coherent island sizes of the three DIP films (32 nm @400 K, 28 nm @300 K, 15 nm @200 K). We therefore conclude that the increase in the FWHM of the DIP HOMO and the DOGS is ascribed to the increase in the density of structural defects.[12] However, the FWHM of the PFP HOMO did not increase as much as that of the DIP although the structural defects of the PFP also increase (see also Figure S2).[22] This can be reasonably understood from the following results and consideration: (i) PFP molecules in an overlayer tend to adopt the orientation of the DIP molecules in the bottom layer, and the crystalline quality of the PFP layer correlates with that of the DIP layer in terms of the in-plane coherent crystal size;[22] (ii) however, PFP domains are larger than DIP domains and thus have a smaller number of domain boundaries, which generally cause many gap states;[32,33] and therefore (iii) there is less HOMO-band broadening and fewer gap states in the PFP than in the DIP, which can not be measured with conventional UPS.[31,32,34]

It is clear from Figure 4 that the energy difference ($E_{H\text{-}H}$) between the PFP HOMO and DIP HOMO decreased with an increase in the defects as it is understood from the lowering of PFP-HOMO energy for the 300-K system ($\Delta E_{1H\text{-}H}$) and the 200-K system ($\Delta E_{2H\text{-}H}$).As shown in **Figure 5**, a systematic relationship between the increase in the defects and the WF shift at the OOH was observed. The increase in WF may be caused by electron transfer from the DIP to the PFP to establish thermal equilibrium, which is related to the change in the electrostatic potential across the interface due to the electron transfer. Moreover, the values of $\Delta E_{1H\text{-}H}$ (0.11 ± 0.02 eV) and $\Delta E_{2H\text{-}H}$ (0.21 ± 0.02 eV) correspond reasonably well with the additional electrostatic

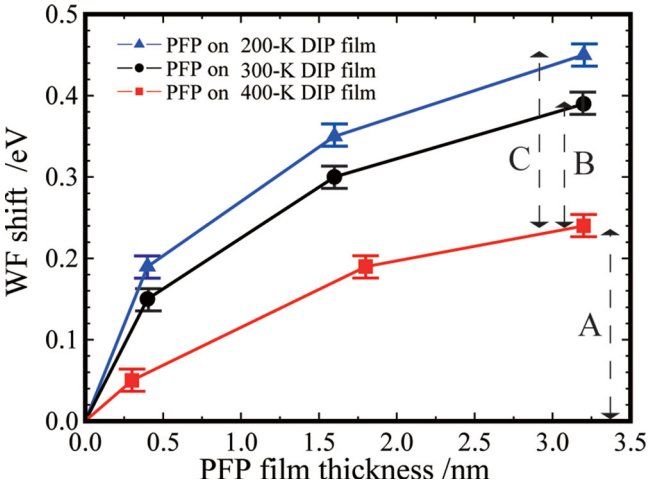

Figure 5. Work function (WF) shift versus PFP film thickness for three DIP films until PFP covers the DIP film surface. "A" denotes the electronic potential change at the lowest defect density interface. "B" and "C" denote additional electronic potential changes induced by an increase of the defect density at the interface.

© 2014 WILEY-VCH Verlag GmbH & Co. KGaA, Weinheim

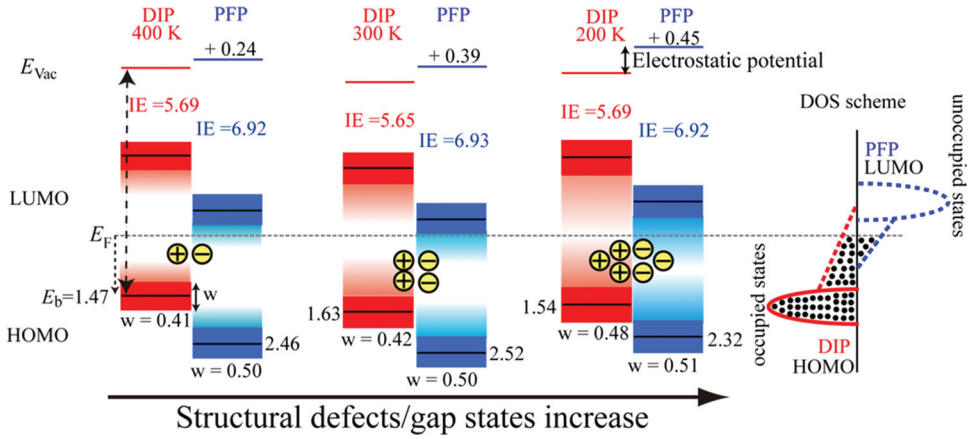

Figure 6. Energy level diagrams of PFP (3.2 nm)-on-DIP (20 nm) heterostructures with different defect densities. Thickness of colored boxes represent width of HOMO and LUMO level with FWHM (w) measured for HOMO (LUMO width assumed to be similar to that for HOMO). Distribution of gap states is shown by shading. Onset-to-onset band gap of 2.55 eV for DIP is taken from a previous report.[35] Band gap for PFP is assumed to be ~2.8 eV by adding 1.0 eV (exciton binding energy of pentacene)[36] to the optical band gap.[37] Different DIP HOMO E_b is presumably due to variation in WF of SiO_2 substrates. Density of states (DOS) scheme is shown on right side. All numbers are given in eV.

potential change (further WF increase), for the 300-K system (B) (0.15 ± 0.02 eV) and the 200-K system (C) (0.21 ± 0.02 eV), respectively. These results indicate that the defect density at the PFP-on-DIP OOH thus the density of gap states increased in both PFP and DIP films near the interface. Therefore, the change in the electrostatic potential across the interface increased due to electron transfer from the occupied gap states in the DIP layer to the unoccupied gap states in the PFP overlayer. As we did not observe any experimental evidence of the charge transfer complex formation, it is more plausible that the excess electrons in the PFP and the excess holes in the DIP are not distributed only among the interface molecules. Accordingly, there are various dipole-like electron-hole pairs near the interface, and, on average they acted phenomenologically as an interface dipole layer (quasi-interface dipole layer), which should be separated in scientific discussion on the interface-related phenomena from the interface dipole by direct electronic interaction only at the interface, as discussed in previous reports.[9,11]

Since the IE was independent of the defect density for both the DIP and PFP films, the decrease in E_{H^-H} (ΔE_{1H^-H} and ΔE_{2H^-H}) together with the increase in the electrostatic potential change (B and C) can be ascribed to moving of the Fermi-level in each band gap.[10,18,31,32] Energy level diagrams of the PFP-on-DIP OOHs are shown in **Figure 6** with the changes in these gap states. The band gap and exciton E_b values are taken from previous reports.[35–37] The ELA of the PFP-on-DIP system is presumably governed by the change in the electrostatic potential across the interface produced by partial electron transfer from DIP HOMO-derived gap states to PFP LUMO-derived gap states, as suggested for other organic donor-accepter interfaces.[10,11] The change in the electrostatic potential depends on the number of transferred electrons and their spatial distribution, which are dominated by the density of gap states in the donor layer (occupied gap states) and acceptor layer (unoccupied gap states) as well as the WF difference before the contact.[10] The electron transfer is not due to electronic interaction but to the achievement of thermal equilibrium, in which the density and energy distribution of defect mediated gap states are important factors for the ELA at the OOH as at a weakly interacting organic-conductor interface.[31,32]

3. Conclusion

We investigated the dependence of the energy level alignment (ELA) on structural defects at a weakly interacting organic heterojunction (OOH) system by using X-ray scattering and UPS. From studying PFP-on-DIP as the model system, we experimentally demonstrated that (i) the ELA depends on the density of structural defects near the interface, (ii) the effect of the defect density on the IE is very small (less than 50 meV), and (iii) the change in the electrostatic potential across the PFP-on-DIP OOH interface greatly depends on the defect density with a variation of more than 200 meV.

From the present study, we conclude that a key factor affecting the ELA at OOH interfaces is the change in the electrostatic potential across the OOH interface, which is produced by partial electron transfer from the donor layer to the acceptor layer, where the structural defects, which result in gap states, play a crucial role. The energy and spatial distribution of the gap states depend strongly on the defects and, more generally, on crystal disorder.[31,32,38] An increased density of gap states due to an increase in the structural defects enables a larger number of electrons to transfer from occupied gap states of donor layer to unoccupied gap states of accepter layer below the Fermi level, which are hardly detectable with conventional UPS instruments. In summary, the ELA at OOH interfaces can be controlled by adjusting the density of structural defects (by e.g. the growth temperature), which is a key technology to control the efficiency and functionality of organic devices employing OOHs, such as OPV cells.

4. Experimental Section

Si(111) wafers with native SiO_2 (surface roughness σ_{rms} = 0.3 nm) were cleaned ultrasonically with acetone, isopropyl alcohol, and ultrapure water, followed by heating to 870 K in the UHV growth chamber,

© 2014 WILEY-VCH Verlag GmbH & Co. KGaA, Weinheim

and used as substrates. DIP thin films were deposited on these SiO_2 substrates under ultrahigh vacuum (UHV) conditions (base pressure $< 8 \times 10^{-8}$ Pa) by thermal evaporation at different substrate temperatures (T = 400, 300, and 200 K), while the PFP films were deposited only at 300 K on those DIP films. The PFP deposition was interrupted a few times for ~1 hour for each time to measure the thickness dependence of the UPS. For both the DIP and PFP, the growth rate was between 0.1 and 1.0 nm/min as determined using a quartz crystal microbalance. After each growth of the PFP films in the UHV preparation chamber, the samples were transferred to the measurement chamber without breaking the vacuum for UPS at 300 K. The DIP films for X-ray scattering measurements were prepared in the same way as for UPS.

He I UPS experiments were performed in situ with a custom-built UHV system equipped with a PHOIBOS-HSA100 analyzer with an energy resolution of 60 meV, a light incident angle of 45°, an electron emission angle of 0° (normal emission), and a photoelectron acceptance angle of ± 9°.[39] The vacuum levels (VLs) were obtained from the SECO of the UPS spectra, for which a sample bias of −5 V was applied. The IE, HOMO E_b, and VL values were obtained by repeated measurements. The error in these values was estimated to be ± 0.01 eV.

GIXD measurements were performed in situ at the X04SA beamline of the Swiss Light Source, Paul Scherrer Institut, Villigen, Switzerland (X-ray wavelength λ = 0.10 nm) to investigate the in-plane structure of the films. The lower limits of the in-plane coherent crystal size l_s were determined using the Scherrer equation ($l_s = 2\pi * \mathrm{FWHM}^{-1} * 0.9394 * K_s$, where K_s = 1.0747 is the Scherrer constant for spherical grains and FWHM is the full width at half maximum of the peak in $Å^{-1}$ determined with a Gaussian fit-function).[40] As the instrumental broadening due to the diffractometer resolution was not included in the calculation, only the lower limits of l_s are given.

Supporting Information

Supporting Information is available online from the Wiley Online Library or from the author.

Acknowledgements

This research has been supported by the Global COE program of MEXT (G03) at Chiba University and Grant-in-Aid for Scientific Research (A) (No. 24245034). A.H. acknowledges support from the Japanese Society for the promotion of Science, and, S.K. acknowledges support from Grant-in-Aid for Scientific Research (B) (No. 23360006). We thank Dr. S.Leake and Dr. P.Willmott at the MS beamline of the Swiss Light Source for experimental support, Dr. A. Gerlach and Dr. K. Broch from Tübingen University for help during synchrotron beamtime and Prof. K. Sakamoto, Dr. F. Bussolotti, Prof. S. Duhm and Dr. R. Suizu for their helpful discussions.

Received: January 3, 2014
Revised: February 28, 2014
Published online:

[1] P. Peumans, A. Yakimov, S. R. Forrest, *J. Appl. Phys.* **2003**, *93*, 3693.
[2] N. Koch, *Chem. Phys. Chem.* **2007**, *8*, 1438.
[3] J. Hwang, A. Wan, A. Kahn, *Mater. Sci. Eng. R* **2009**, *64*, 1.
[4] S. Olthof, R. Meerheim, M. Schober, K. Leo, *Phys. Rev. B* **2009**, *79*, 245308.
[5] C. J. Brabec, A. Cravino, D. Meissner, N. S. Sariciftci, T. Fromherz, M. T. Rispens, L. Sanchez, J. C. Hummelen, *Adv. Funct. Mater.* **2001**, *11*, 374.
[6] S. E. Gledhill, B. Scott, B. A. Gregg, *J. Mater. Res.* **2005**, *20*, 3167.
[7] A. Gadisa, M. Svensson, M. R. Andersson, O. Inganas, *Appl. Phys. Lett.* **2004**, *84*, 1609.
[8] A. C. Morteani, P. Sreearunothai, L. M. Herz, R. H. Friend, C. Silva, *Phys. Rev. Lett.* **2004**, *92*, 247402.
[9] H. Fukagawa, S. Kera, T. Kataoka, S. Hosoumi, Y. Watanabe, K. Kudo, N. Ueno, *Adv. Mater.* **2007**, *19*, 665.
[10] H. Y. Mao, F. Bussolotti, D. C. Qi, R. Wang, S. Kera, N. Ueno, A. T. S.Wee, W. Chen, *Org. Electron.* **2011**, *12*, 534.
[11] Z. L. Guan, J. B. Kim, Y. L. Loo, A. Kahn, *J. Appl. Phys.* **2011**, *110*, 043719.
[12] T. Hosokai, H. Machda, S. Kera, A. Gerlach, F. Schreiber, N. Ueno, *Phys. Rev. B* **2011**, *83*, 195310.
[13] S. Braun, W. R. Salaneck, M. Fahlman, *Adv. Mater.* **2009**, *21*, 1450.
[14] H. Vazquez, W. Gao, F. Flores, A. Kahn, *Phys. Rev. B* **2005**, *71*, 041306.
[15] M. Linares, D. Beljonne, J. Cornil, K. Lancaster, J. L. Brédas, S. Verlaak, A. Mityashin, P. Heremans, A. Fuchs, C. Lennartz, J. Ide, R. Mereau, P. Aurel, L. Ducasse, F. Castet, *J. Phys. Chem. C* **2010**, *114*, 3215.
[16] J. Ivanco, *Thin Solid Films* **2012**, *520*, 3975.
[17] S. Duhm, G. Heimel, I. Salzmann, H. Glowatzki, R. L. Johnson, A. Vollmer, J. P. Rabe, N. Koch, *Nat. Mater.* **2008**, *7*, 326.
[18] S. Zhong, J. Q. Zhong, H. Y. Mao, J. L. Zhang, J. D. Linb, W. Chen, *Chem. Chem. Phys.* **2012**, *14*, 14127.
[19] T. W. Ng, M. F. Lo, S. T. Lee, C. S. Lee, *Org. Electron.* **2012**, *13*, 1641.
[20] J. Puigdollers, A. Marsal, S. Cheylan, C. Voz, R. Alcubilla, *Org. Electron.* **2010**, *11*, 1333.
[21] A. Hinderhofer, T. Hosokai, K. Yonezawa, A. Gerlach, K. Kato, K. Broch, C. Frank, J. Novak, S. Kera, N. Ueno, F. Schreiber, *Appl. Phys. Lett.* **2012**, *101*, 033307.
[22] A. Hinderhofer, T. Hosokai, C. Frank, J. Novak, A. Gerlach, F. Schreiber, *J. Phys. Chem. C* **2011**, *115*, 16155.
[23] A. Hinderhofer, F. Schreiber, *Chem. Phys. Chem.* **2012**, *13*, 628.
[24] M. A. Heinrich, J. Paum, A. K. Tripathi, W. Frey, M. L. Steigerwald, T. Siegrist, *J. Phys. Chem. C* **2007**, *111*, 18878.
[25] A. C. Dürr, F. Schreiber, K. A. Ritley, V. Kruppa, J. Krug, H. Dosch, B. Struth, *Phys. Rev. Lett.* **2003**, *90*, 016104.
[26] S. Kowarik, A. Gerlach, S. Sellner, F. Schreiber, L. Cavalcanti, O. Konovalov, *Phys. Rev. Lett.* **2006**, *96*, 125504.
[27] S. Kowarik, A. Gerlach, S. Sellner, L. Cavalcanti, O. Konovalov, F. Schreiber, *Appl. Phys. A* **2009**, *95*, 233.
[28] Y. L. Huang, W. Chen, H. Huang, D. C. Qi, S. Chen, X. Y. Gao, J. Paum, A. T. S. Wee, *J. Phys. Chem. C* **2009**, *113*, 9251.
[29] J. Wagner, M. Gruber, A. Hinderhofer, A. Wilke, B. Bröker, J. Frisch, P. Amsalem, A. Vollmer, A. Opitz, N. Koch, F. Schreiber, W. Brütting, *Adv. Funct. Mater.* **2010**, *20*, 4295.
[30] I. Salzmann, S. Duhm, G. Heimel, M. Oehzelt, R. Kniprath, R. L. Johnson, J. P. Rabe, N. Koch, *J. Am. Chem. Soc.* **2008**, *130*, 12870.
[31] T. Sueyoshi, H. Kakuta, M. Ono, K. Sakamoto, S. Kera, N. Ueno, *Appl. Phys. Lett.* **2010**, *96*, 093303.
[32] F. Bussolotti, S. Kera, K. Kudo, A. Kahn, N. Ueno, *Phys. Rev. Lett.* **2013**, *110*, 267602.
[33] R. Matsubara, N. Ohashi, M. Sakai, K. Kudo, M. Nakamura, *Appl. Phys. Lett.* **2008**, *200892*, 242108.
[34] A. Hinderhofer, A. Gerlach, K. Broch, T. Hosokai, K. Yonezawa, K. Kato, N. Ueno, F. Schreiber, *J. Phys. Chem. C* **2013**, *117*, 1053.
[35] A. Wilke, J. Endres, U. Hörmann, J. Niederhausen, R. Schlesinger, J. Frisch, P. Amsalem, J. Wagner, M. Gruber, A. Opitz, A. Vollmer, W. Brütting, A. Kahn, N. Koch, *Appl. Phys. Lett.* **2012**, *101*, 233301.
[36] R. Schuster, M. Knupfer, H. Berger, *Phys. Rev. Lett.* **2007**, *98*, 037402.
[37] A. Hinderhofer, U. Heinemeyer, A. Gerlach, S. Kowarik, R. M. J. Jacobs, Y. Sakamoto, T. Suzuki, F. Schreiber, *J. Chem.Phys.* **2007**, *127*, 194705.
[38] Y. S. Huang, S. Westenhoff, I. Avilov, P. Sreearunothai, J. M. Hodgkiss, C. Deleener, R. H. Friend, D. Beljonne, *Nat. Mater.* **2008**, *7*, 483.
[39] T. Hosokai, M. Horie, T. Aoki, S. Nagamatsu, S. Kera, K. K. Okudaira, N. Ueno, *J. Phys. Chem. C* **2008**, *112*, 4643.
[40] M. Birkholz, *Thin Film Analysis by X-Ray Scattering*, Wiley-VCH, Weinheim, Germany, **2006**.

© 2014 WILEY-VCH Verlag GmbH & Co. KGaA, Weinheim